Journal of Alloys and Compounds 546 (2013) 28–40

Contents lists available at SciVerse ScienceDirect

Journal of Alloys and Compounds

journal homepage: www.elsevier.com/locate/jalcom

Effects of heat treatment on microstructure and mechanical properties of ZW21 magnesium alloy

T.J. Chen *, W. Wang, D.H. Zhang, Y. Ma, Y. Hao

Key Laboratory of Gansu Advanced Nonferrous Metal Materials, Lanzhou University of Technology, Lanzhou 730050, China

ARTICLE INFO

Article history:
Received 22 June 2012
Received in revised form 14 August 2012
Accepted 15 August 2012
Available online 28 August 2012

Keywords:
ZW21 magnesium alloy
Heat treatment
Microstructure
Mechanical properties
Fracture regime

ABSTRACT

The effects of heat treatment on the microstructure and mechanical properties of a ZW21 magnesium alloy are investigated. The results indicate that the interdendritic eutectic W phase with discontinuous laths and large-sized pools in the as-cast ZW21 alloy is harmful to its mechanical properties. But heat treatment including solution and subsequent aging can change the amount, size, morphology and distribution of the W phase, and thus can improve the mechanical properties. The treatment technique of solution at 525 °C for 4 h and subsequent aging at 250 °C for 24 h is appropriate for this alloy and can increase the ultimate tensile strength, elongation and hardness from 205 MPa, 18.25% and 50 HV of the as-cast alloy to 243 MPa, 23.75% and 68.7 HV, respectively. The fracture regimes such as quasi-cleavage or cleavage and the proportion of grain debonding in crack propagation also change with the treatment parameters. All of these changes are attributed to the variation of deformation harmony resulted from composition homogenization, grain growth and MgSnCa particle coarsening, or/and grain bonding strength determined by the distribution of W phase.

1. Introduction

As the lightest metallic structural materials, magnesium alloys have great application potential in the fields of automobile and aerospace [1]. Unfortunately, the mechanical properties of the commonly used magnesium alloys are relatively low and cannot match the requirements in many application conditions. However, it has been reported that wrought Mg–Zn–Y alloys exhibit significantly improved mechanical properties at room temperature as well as at elevated temperatures [2]. A $Mg_{97}Y_2Zn_1$ (in mol%) alloy produced by rapid solidified powder metallurgy exhibits a yield stress of more than 610 MPa and elongation of 5% at room temperature and a yield strength more than 380 MPa at 200 °C [3]. As-cast monolithic Mg–Zn–Y alloys have yield stress from 180 to 480 MPa at room temperature, depending on their compositions [4]. So Mg–Zn–Y system is an ideal candidate for developing new magnesium alloys with high performance.

The authors have developed a new Mg–Zn–Y alloy named ZW21 through orthogonal experiment method [5]. It has the ultimate tensile strength of 205 MPa and elongation of 18.25%. The total content of high-cost RE elements is only 1.5% (1% Y and 0.5% Nd) and the Zn concentration is about 2%. So this alloy has higher mechanical properties, lower cost and lighter weight compared with the other commonly-used congeneric alloys. Nd has similar roles to Y in Mg–Zn–Zr alloys and can partially replace Y in ternary Mg–Zn–Y phases [6,7]. This alloy also contains 0.5% Sn, 0.3% Zr and 0.05% Ca. The element of Sn does not only improve the castability of magnesium alloys, but also more importantly can form Mg_2Sn precipitates during solution-aging treatment to enhance mechanical properties [8]. Zr element is used as a grain refiner in Mg–Zn alloys and exists in pure Zr particles that can act as the nucleation substrates of α-Mg [9]. Ca has significant grain refinement besides reducing the oxidation of magnesium alloy melts, especially, 0.2% Ca has good effect on improving UTS and yield strength of Mg–Zn–RE alloys [10,11]. The Sn-, Zr- and Ca-riched phases are quite limited because the concentrations of these three elements are very low. So the main phase should be the Mg–Zn–Y (Nd) phase in the ZW21 alloy [5].

In general, there are three kinds of ternary equilibrium phases in the Mg–Zn–Y system alloys, i.e. I phase (Mg_3Zn_6Y, icosahedral quasicrystal structure, quasi-periodically ordered), W phase ($Mg_3Zn_3Y_2$, cubic structure) and Z or X phase ($Mg_{12}ZnY$) [3]. The I or Z phase is closely bonded with the Mg matrix and can effectively retard the basal slip, thereby strengthens the alloy greatly [2–4,12–17]. But the W phase is easy to crack during tensile testing and the interfaces of W phase with Mg matrix are not coherent because of the limited symmetry of these phases, and thus the W phase containing alloys have relatively low mechanical properties [4,18–22]. However, also some investigations indicate that the W phase is beneficial for improving mechanical properties: the W phase can increase the ductility [4]; when the volume fraction of

* Corresponding author. Tel.: +86 931 2976573; fax: +86 931 2976578.
E-mail addresses: chentj1971@126.com, chentj@lut.cn (T.J. Chen).

0925-8388/$ - see front matter © 2012 Elsevier B.V. All rights reserved.
http://dx.doi.org/10.1016/j.jallcom.2012.08.058

W phase is between 11.2% and 17.5%, the alloys have superior strength due to the strong bonding interface between W phase and Mg matrix [23]; the alloys containing W + Z phases always exhibit higher comprehensive mechanical properties than those containing unique I or Z phase [19,20]. That is to say there is a dispute for the effects of W phase on the mechanical properties. The authors' previous investigation indicated that the ZW21 alloy only had one Mg–Zn–Y(Nd) phase, the W phase ($Mg_3Zn_3(Y, Nd)_2$) [5]. Then a problem arises that what a role the W phase plays in the ZW21 alloy.

In addition, the heat treatment behaviors of Mg–Zn–Y alloys, especially the effects of heat treatment on microstructure and mechanical properties, are not clear. Most of the existing investigations on this aspect only involve the effects of a given treating parameter on the microstructures and mechanical properties of the as-cast and deformed (rolled or extruded) alloys [2,14,24,25]. The detailed effects of each of parameters such as the solution temperature and time prior to deformation and annealing temperature and time after deformation are not systematically studied. Only two papers have involved the effects of annealing time at given temperatures after deformation of a I-phase and a W-phase containing magnesium alloys respectively [16,17]. The investigation on the heat treatment behaviors of as-cast alloys has not been found.

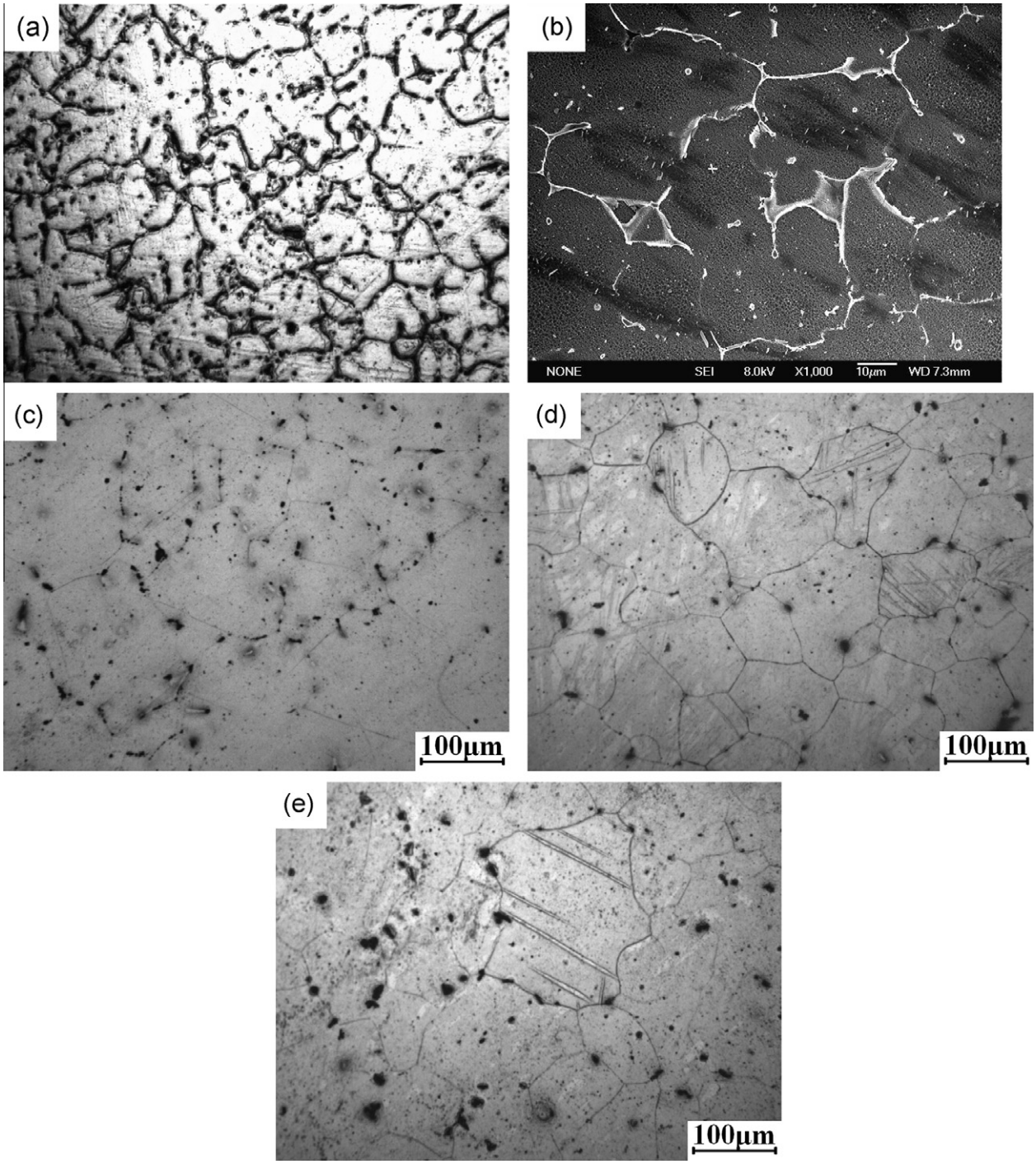

Fig. 1. Microstructures of the ZW21 alloys solutionized for 12 h at different temperatures. (a) and (b) room temperature (as-cast), (c) 505 °C, (d) 525 °C and (e) 545 °C.

So it can be concluded that the effects of W phase on the microstructures and mechanical properties of Mg–Zn–Y alloys and their heat treatment behaviors are still unclear. More particularly, all of these problems have not involved for the ZW21 alloy. To verify these problems, the ZW21 alloy was solutionized at different temperatures for 12 h and at 525 °C for different times to study the effects of solution temperature and solution time respectively. The alloy solutionized at 525 °C for 4 h was subsequently aged at 250 °C for different durations to study the effect of aging time. The corresponding microstructures and fracture regimes during tensile testing were detailedly investigated.

2. Experimental procedure

The composition of the ZW21 alloy is Mg–2Zn–1Y–0.5Nd–0.5Sn–0.3Zr–0.05Ca. The alloy was prepared using Mg, Zn, Sn and Ca pure metals, and Mg–30Zr, Mg–30Y and Mg–30Nd master alloys. During melting, JDMJ refine agent and a special covering agent for Mg–RE alloys were employed. The prepared melts were finally poured into a permanent mold with a cavity of Φ16 mm × 110 mm at 710–720 °C. To verify the effect of solution temperature on the alloy's microstructure and mechanical properties, some of the rods were solutionized for 12 h at 505 °C, 525 °C and 545 °C respectively. The other rods were solutionized at 525 °C for different times ranging of 0.5–72 h to examine the effect of solution time. The rods solutionized for 4 h were aged at 250 °C for different times ranging of 2–72 h to investigate the age behavior of the alloy. All of the heat treated rods were water-quenched and then machined into tensile bars with a gauge of 40 mm and a diameter of 8 mm. The water temperature for quenching was the room temperature (about 25 °C). All of the tensile bars were cut from the center sections of the rods. The tensile test was carried out on a universal testing machine at a strain rate of 1.67×10^{-3} s^{-1}. The average of at least three tests was taken as the final mechanical properties for each alloy.

Metallographic specimens were cut from the as-cast and heat treated rods, and finished and polished by standard metallographic technique. The as-cast and aged specimens were etched by an aqueous solution containing picric acid, acetic acid and ethanol. The solutionized specimens were etched by an aqueous solution containing nitric acid. Then they were observed by an optical microscope (OM) and a scanning electron microscope (SEM). The phase constituents of the alloys were examined by an X-ray diffractometer (XRD) and the compositions of some phases were analyzed by an energy disperse spectroscopy (EDS). Some specific alloys were examined by a differential thermal analyzer (DTA) in a heating rate of 10 °C min^{-1}. The fracture surfaces and their side-views were also observed on the SEM and OM respectively.

3. Results and discussion

3.1. Effects of solution temperature

As shown by Fig. 1a, the as-cast microstructure of the ZW21 alloy is composed of small equiaxed dendrites (the grain size is about 50 μm) and the net-like interdendritic eutectic structures (Fig. 1a). The distribution of eutectic W is not continuous and it exists in discontinuous laths in the thin regions between the dendrites and in pools in the triangle regions (Fig. 1b). After being solutionized at 505 °C for 12 h, the interdendritic net-like eutectic structures are still visible (Fig. 1c), which implies that a quite large amount of W phase does not dissolve. This is consistent with the result of XRD, the peaks of W phase can be detected (Fig. 2). As the temperature is elevated to 525 °C or above, the net-like structures disappear and only some particles sporadically distribute at the grain boundaries (Fig. 1d and e). But the XRD result indicates that there is no W phase at these temperatures (Fig. 2). This implies that the W phase has basically completely decomposed. The DTA result of the alloy heated at 525 °C for 4 h shows that there is only one endothermic peak corresponding to the melting of α-Mg (Fig. 3). So these particles should be other one or more phases with high thermal stability. However, the XRD does not verify them probably due to their minor amount. In addition, it can be found that both the grains and particles have obviously grown up when the temperature is elevated from 525 °C to 545 °C, and some particles enter into the coarsened grains due to the grain mergence (comparing Fig. 1d and e).

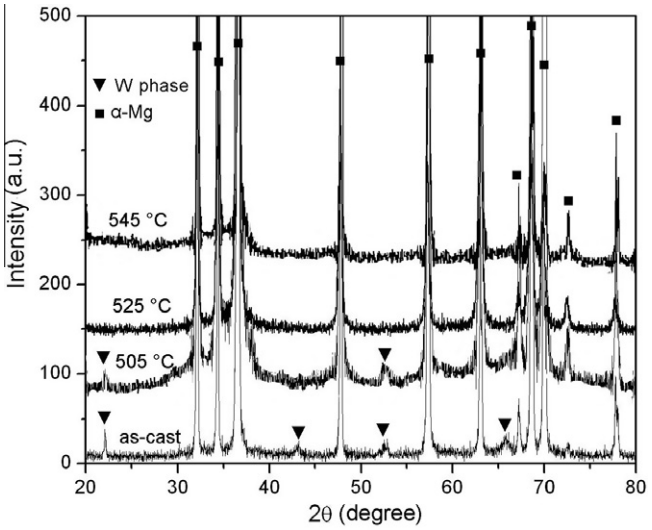

Fig. 2. XRD diffractograms of the ZW21 alloy heated for 12 h at different temperatures.

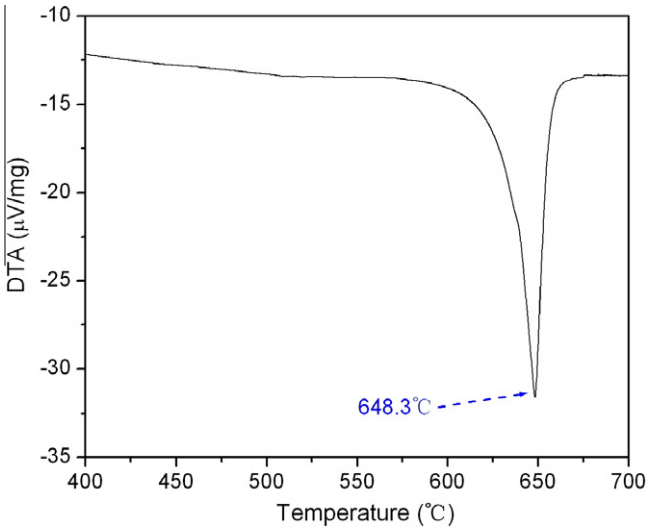

Fig. 3. DTA curve of the ZW21 alloy solutionized for 4 h at 525 °C.

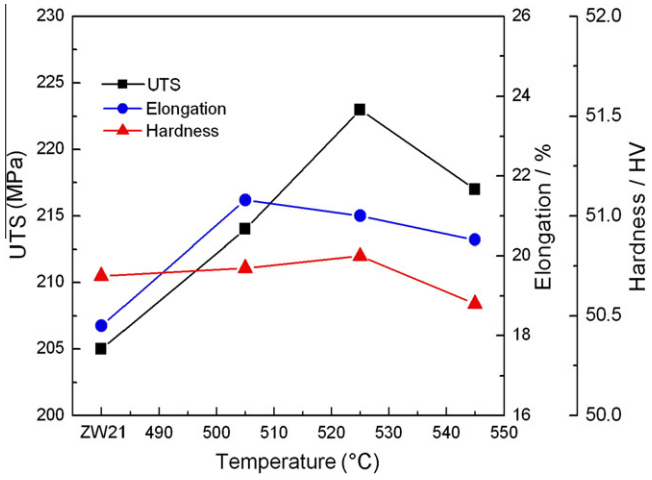

Fig. 4. Variations of mechanical properties of the ZW21 alloy with solution temperature.

The investigation on Mg–Sn–Sr alloys indicates that the dissolution temperature of Mg_2Sn phase is ~406 °C [26]. The Mg_2Sn phase can completely dissolve into the α-Mg phase when a Mg–4Al–2Sn–1Ca alloy is solutionized for 4 h at 520 °C [11] or Mg–5Sn–(0.3–3.3Sr) alloys are heated for 24 h at 500 °C [26]. So it is reasonably expected that the Mg_2Sn phase in the as-studied ZW21 alloy should have completely dissolved when the alloy is solutionized for 12 h at 525 °C or 545 °C. The particles thereby are not the Mg_2Sn phase. It is known that adding Ca or Sr into Mg–Sn alloys is a promising way for developing creep-resistant magnesium alloys because a new phase of MgSnCa or MgSnSr with good thermal stability can form [27]. The dissolution temperature of MgSnSr phase is up to ~555 °C and its particle size and morphology almost do not change after the alloys are solutionized at 500 °C for 24 h [26]. For the Mg–4Al–2Sn–1Ca, the MgSnCa particles can still be obviously observed after the alloy is heated for 4 h at 520 °C [28]. The result from electron probe microanalyzer indicates that MgSnCa phase particles really exist in the interdendritic regions of the as-cast ZW21 alloy and these particles do not contain other elements such as Y, Nd and Zr [5]. In addition, the other secondary phases are not found except the W, Mg_2Sn, MgSnCa and pure Zr particles. The Zr particles exist in the center of primary grains and their size is very small [5]. So it can be proposed that the black particles in the microstructures shown by Fig. 1d and e should be the MgSnCa phase. Moreover, the MgSnCa particles will coarsen driving by decreasing the MgSnCa/α-Mg interfacial energy as the temperature rises, which can be demonstrated by comparing Fig. 1d and e.

Fig. 4 gives the variations of hardness, UTS and elongation of the ZW21 alloy with the solution temperature. It shows that the three properties all increase after the alloy is solutionized at 505 °C for 12 h compared with those of the as-cast alloy. As the temperature rises, the UTS and hardness further increase, but the elongation decreases. When the temperature exceeds 525 °C, the three properties all decrease. The alloy heated at 525 °C has the highest comprehensive mechanical properties, the UTS of 223 MPa, elongation of 21% and hardness of 50.6 HV. It should be noted that the change range of the hardness is very small although it changes with the solution temperature.

Most of the W phase in the as-cast ZW21 alloy distributes in the form of laths at grain boundaries (Fig. 1b). The W phase with such distribution and morphology is easy to crack during tensile testing [4,17–22]. The solution treatment leads the W phase to dissolve into the α-Mg phase and thus decrease the crack initiation sites. Simultaneously, the solution strengthening is also enhanced due to the dissolution of W phase. So the mechanical properties of the alloy heated at 505 °C are improved. As the solution temperature rises, the amount of dissolved W phase increases and the solution strengthening is further enhanced, and thus both the UTS and hardness continuously increase. But it is known that solution strengthening always impair the deformability of an alloy. So the elongation decreases as the temperature rises. In addition, the UTS and hardness also decrease when the temperature exceeds 525 °C due to the grain growth.

Fig. 5 shows the fracture surface morphologies of the ZW21 alloys solutionized at different temperatures. It reveals that there are quite large numbers of cleavage facets besides many small-sized dimples on the surface of the as-cast alloy (Fig. 5a), i.e., the fracture of the as-cast alloy belongs to quasi-cleavage regime. Furthermore, lots of deep cracks are also clearly observed (marked by arrows in Fig. 5a). From the side-view of fracture surface shown by Fig. 6a, it

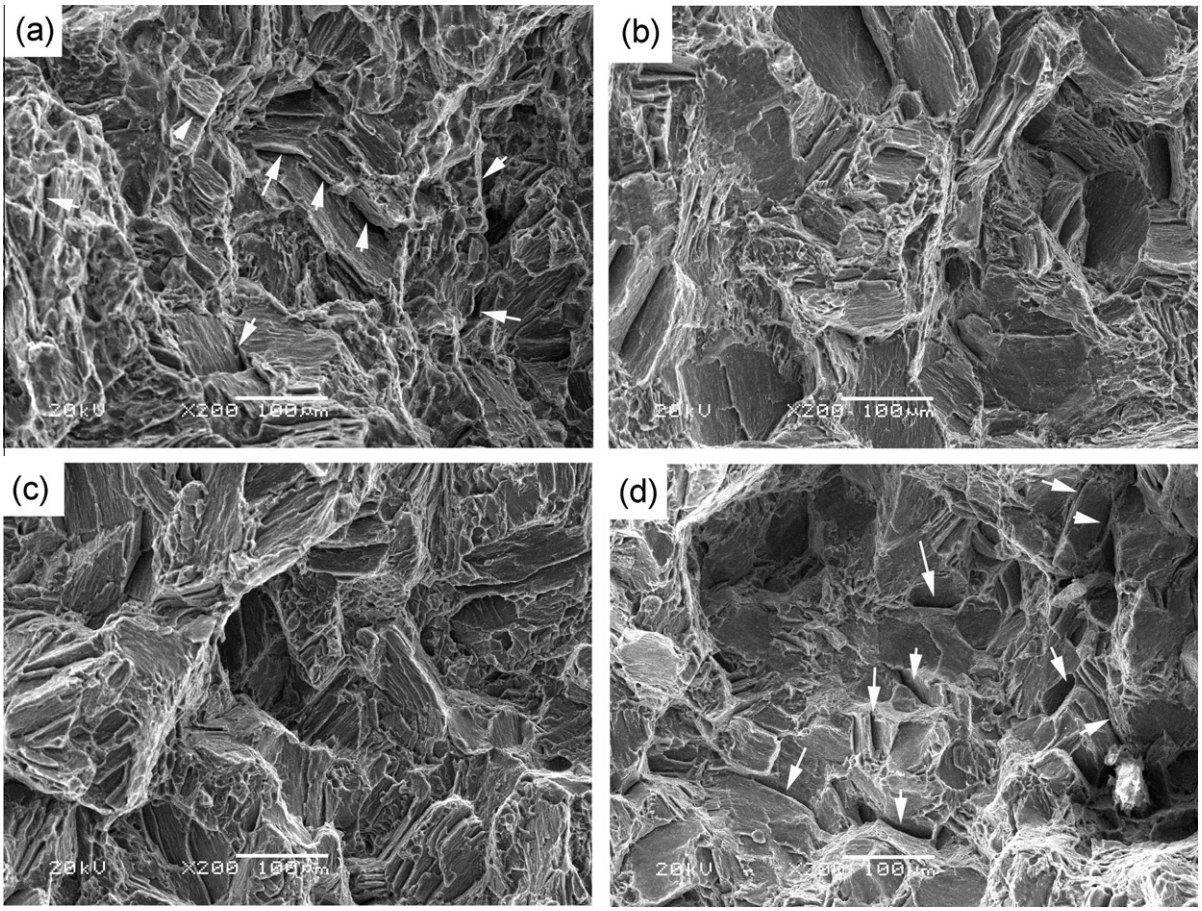

Fig. 5. Fractographs of the ZW21 alloys solutionized for 12 h at different temperatures. (a) as-cast, (b) 505 °C, (c) 525 °C and (d) 545 °C.

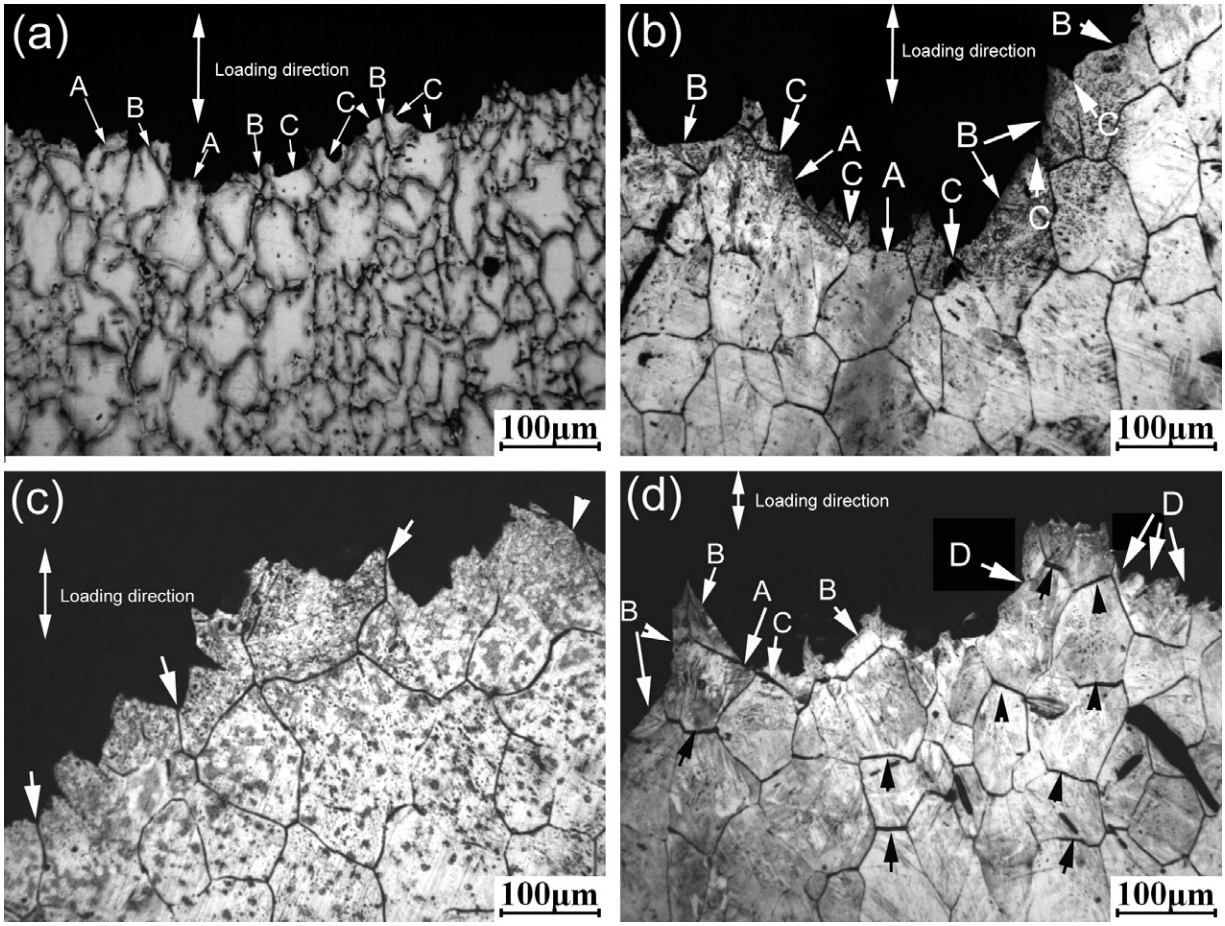

Fig. 6. Microstructures taken near the fracture surfaces along longitudinal direction of the tensile bars of the ZW21 alloys solutionized for 12 h at different temperatures. (a) as-cast, (b) 505 °C, (c) 525 °C and (d) 545 °C.

can be found that the debonding sites of grain boundaries are quite few (marked by A) and cracks more frequently propagate across the grains (marked by arrows C). The sites produced by transgranular fracture always appear in the form of straight lines (shown by arrows C). These straight lines should correspond to the cleavage facets shown in Fig. 5a. In addition, as shown by arrows B in Fig. 6a, there are lots of small cracks along the interdendritic structures, which should correspond to the deep cracks in Fig. 5a. Together with the results from the existing investigations [4,17–22], it can be proposed that cracks initiate in the interdendritic W phase due to its fragile characteristic, and then propagate frequently across the grains. This means that the weak point of the alloy is not the interface of W/α-Mg, but is the W phase itself. This standpoint is not consistent to that from Xu's early study, the W/α-Mg interfaces may easily debond because of the incoherency bonding between them [4], but is identical with that from his latter investigation, cracks are seen in the coarse W phase and the debonding of W/α-Mg interface is not observed [23]. Therefore, it can be proposed that the W phase should be an ideal strengthening phase if it distributes in small particles in the interdendritic regions of the as-cast alloy or dispersively distributes in the grains of the deformed (such as rolled, extruded or equal channel angular processed) alloy or heat treated alloy. Zhang's investigation on a W phase containing Mg–Zn–Y–Zr alloy indicates that its tensile strength is significantly enhanced after being extruded at a high temperature [29]. The reason is that the as-cast W phase pockets are destroyed and fine, dispersive W precipitates form during extrusion.

For the alloy solutionized at 505 °C, the fracture surface is mainly occupied by large-sized cleavage facets and the proportion of dimples is quite little (Fig. 5b), i.e., the fracture of this alloy belongs to cleavage regime. This is just consistent with the result from Fig. 6b, the outline of the fracture surface side-view is basically composed of long straight lines. Grain debonding can be seen occasionally (marked by A in Fig. 6b) and transgranular mechanism absolutely dominates the fracture regime (marked by B). Similarly, there are lots of deep cracks in the fracture surface (Fig. 5b) and they also result from the local grain debonding (marked by C in Fig. 6b). As shown by Fig. 1c, the interdendritic discontinuous net-like eutectic structures are still visible in this state alloy. So it can be expected that its fracture process is similar to that of the as-cast alloy, cracks initiate in the residual W phase and develop across the grains.

As the solution temperature is elevated to 525 °C, cleavage facets on the resulting fracture surface obviously become smaller and dimple characteristics become more obvious compared with the alloy heated at 505 °C (comparing Fig. 5c and b). The general morphology is something like to that of the as-cast alloy (comparing Fig. 5c and a). Namely, its fracture also belongs to quasi-cleavage regime. Fig. 6c shows that only several small-sized sites are related to grain debonding (marked by arrows) and the whole outline almost results from transgranular fracture. By now it can be concluded that the proportion of grain debonding decreases as the temperature rises due to the dissolution of interdendritic W phase. It is further demonstrated that the morphology and

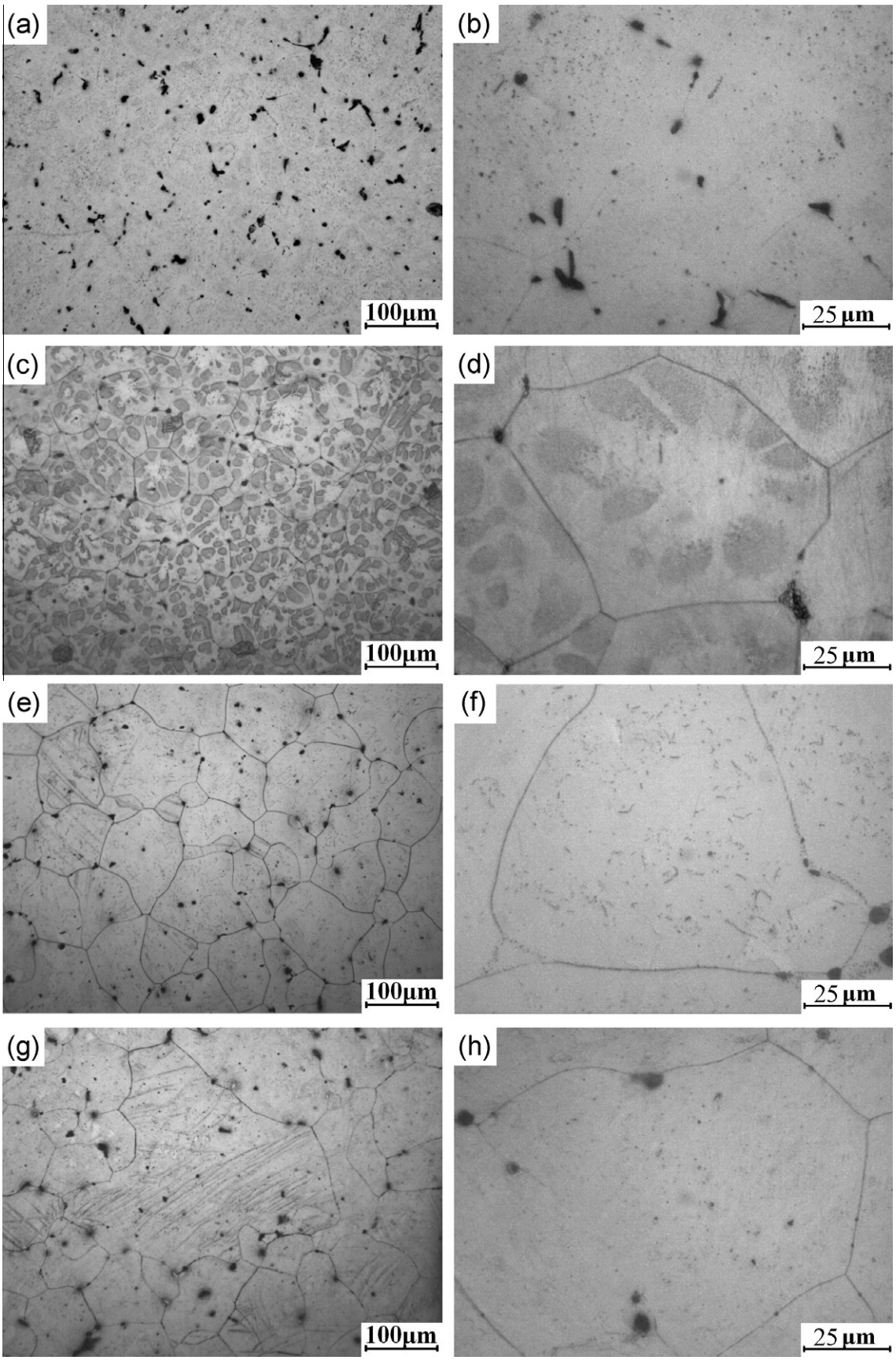

Fig. 7. Microstructures of the ZW21 alloys solutionized at 525 °C for (a) and (b) 0.5 h, (c) and (d) 1 h, (e) and (f) 4 h, (g) and (h) 16 h.

distribution of eutectic W phase in the as-cast alloy are harmful for tensile properties because such W phase is easy to result in grain debonding.

At the solution temperature of 545 °C, cleavage facets dominate the fracture surface again and the surface is in a sugar crystal-like morphology that is composed of polygonal particles (Fig. 5d). In addition, there is always a deep crack between the neighboring particles (marked by arrows). As it is expected, the outline of the surface side-view is almost composed of long straight lines (Fig. 6d), i.e., the alloy fractures in a cleavage form. The deep cracks partially result from the local grain debonding (marked by C), but most of them are the cuneated grooves originated from transgranular fracture (marked by D). Fig. 6d also shows that the fracture belongs to transgranular regime (marked by B) and the proportion of intergranular fracture is quite scarce (marked by A). Furthermore, the grain boundaries perpendicular to the loading direction are obviously wider than those in the other directions, which implies that these boundaries possibly have debonded. But in fact, the intergranular fracture only presents a small proportion. This indicates that the grain bonding is quite strong and it is difficult to debond in large area. Only local sites with small size occasionally debond during tensile testing. For the as-cast alloy and the solutionized alloy at 505 °C, the debonding is attributed to the W phase, but for the alloy treated at 545 °C, the debonding may be ascribed to the coarsened interdendritic MgSnCa particles (Fig. 1e). The latter will be discussed in elsewhere.

Based on the above discussion, it can be concluded that the coarse interdendritic net-like W phase in the as-cast ZW21 alloy is harmful to its tensile properties. Solution treatment can lead the W phase to dissolve into the α-Mg matrix and thus a proper solution treatment can improve the tensile properties. The UTS continuously increases as the solution temperature rises due to the decrease of the W phase amount and size. However, the elongation is impaired because of the solution strengthening. When the temperature exceeds 525 °C, the UTS also decreases due to the coarsening of the primary grains and interdendritic MgSnCa particles. The bonding strength of W/α-Mg interfaces is quite strong and the interface debonding rarely occurs. So cracks always initiate from the W phase and may propagate along this phase. But the fracture is dominated by transgranular regime, and the intergranular fracture due to the prorogation of cracks along the W phase is only in a small proportion. The proportion of intergranular fracture further decreases as the solution temperature rises because the amount and size of the residual W phase are decreased. The whole fracture surface is completely characterized by transgranular regime when the temperature is elevated to 525 °C. But as the temperature is further elevated, the local intergranular fracture appears again possibly due to the coarsened MgSnCa particles at these sites. The fracture of the as-cast alloy belongs to quasi-cleav-

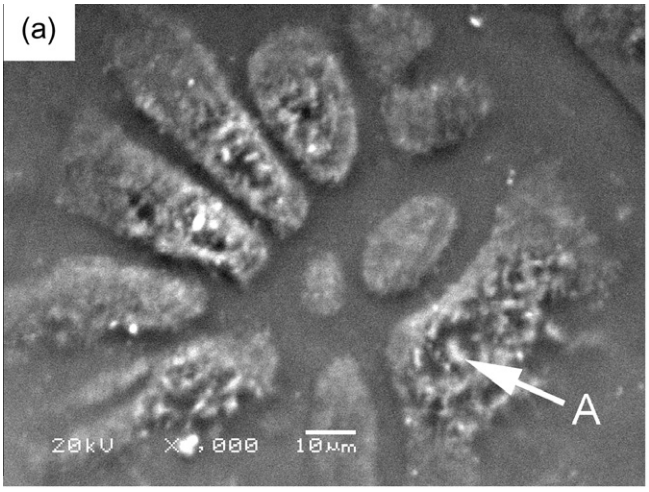

Fig. 9. (a) SEM micrograph of the ZW21 alloy solutionized at 525 °C for 1 h and (b) EDS analysis of the precipitate particle marked by A in (a).

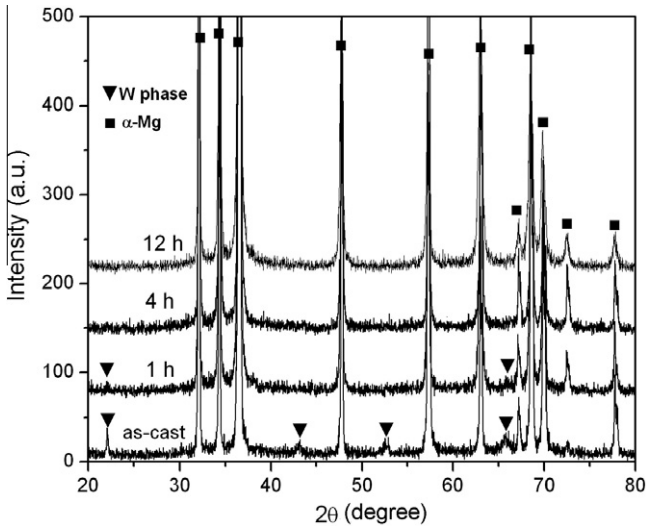

Fig. 8. XRD diffractograms of the ZW21 alloys heated at 525 °C for different durations.

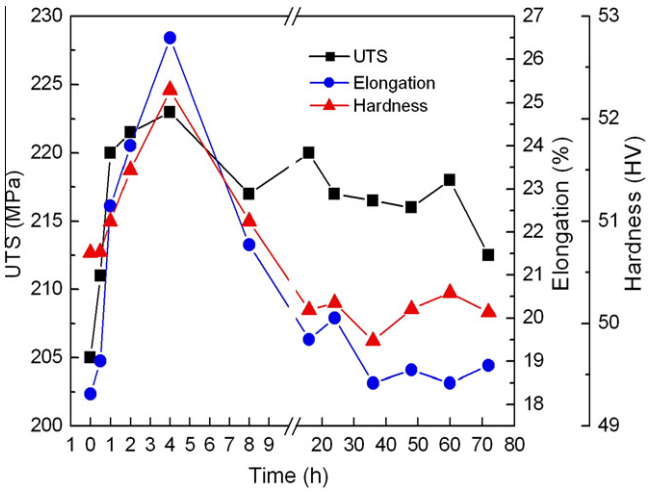

Fig. 10. Variations of mechanical properties of the ZW21 alloy with solution time.

age regime and it changes to cleavage fracture after being solutionized at 505 °C due to solution strengthening. As the solution temperature rises to 525 °C, the composition homogeneity is further improved and the harmfulness from the W phase is eliminated because all of the W phase has completely dissolved, and thus the deformation harmony is mended and the fracture mode again turns into quasi-cleavage regime with obvious dimples. When the temperature is elevated to 545 °C, the fracture mode then changes back to complete cleavage because of the coarsening of the primary grains and MgSnCa particles.

3.2. Effects of solution time

The interdendritic W phase has completely dissolved into the α-Mg matrix and both the primary grains and MgSnCa particles have not obviously coarsened after the ZW21 alloy is solutionized at 525 °C for 12 h. Especially, the resulting tensile properties are the highest among the alloys heated at different temperatures. So the temperature of 525 °C is a suitable solution temperature and in this section, the temperature of 525 °C is employed to study the effects of solution time on the microstructure and tensile properties.

Fig. 7 gives the microstructures of the alloys heated at 525 °C for different durations. It shows that the microstructure of the alloy heated for 0.5 h is similar to that of the alloy heated at 505 °C for 12 h, most of the W phase has dissolved and only some particle-like structures are left (Fig. 7a and b). As the time is increased to 1 h, most of the particle-like structures disappear, but a flower-shaped structure forms in each grain (Fig. 7c). The XRD result shows that the alloy only has a given amount of W phase besides the α-Mg (Fig. 8). But most of the original interdendritic W phase has dissolved at this time. So it can be suggested that the flower-shaped structures may be composed of W phase and this kind of W phase should newly form during solution. The petals of the flower-shaped structures are consisted of small particle (Fig. 9a) and the particles are rich in Zn, Y and Nd elements (Fig. 9b). The atomic ratio of RE/Zn is close to 2:3, which is just consistent with the RE/Zn ratio of W phase. This more directly demonstrates that the flower-shaped structures are composed of W phase. Figs. 7c and 9a shows that the petals in a flower-shaped structure are separate each other and distribute in a radial direction from the grain center. As shown by Fig. 1a, the microstructure of the as-cast ZW21 alloy is composed of small equiaxed dendrites and the dendrite arms in a grain are separated by interdendritic eutectic structure (Fig. 1a). Namely, the eutectic structures in the outline of a grain are separated each other by the dendrite arms. In view of the morphologies of the eutectic structures and the flower-shaped structure, it can be deduced that the sites where the petals distribute should be the sites where the eutectic structures exist. During solution treatment, the eutectic W phase decomposes and transforms into α-Mg solid solution. The diffusion of Y and Nd atoms in the α-Mg matrix is very slow due to their radii are much larger than that of Mg atom [6,7]. So the eutectic W phase structures can-

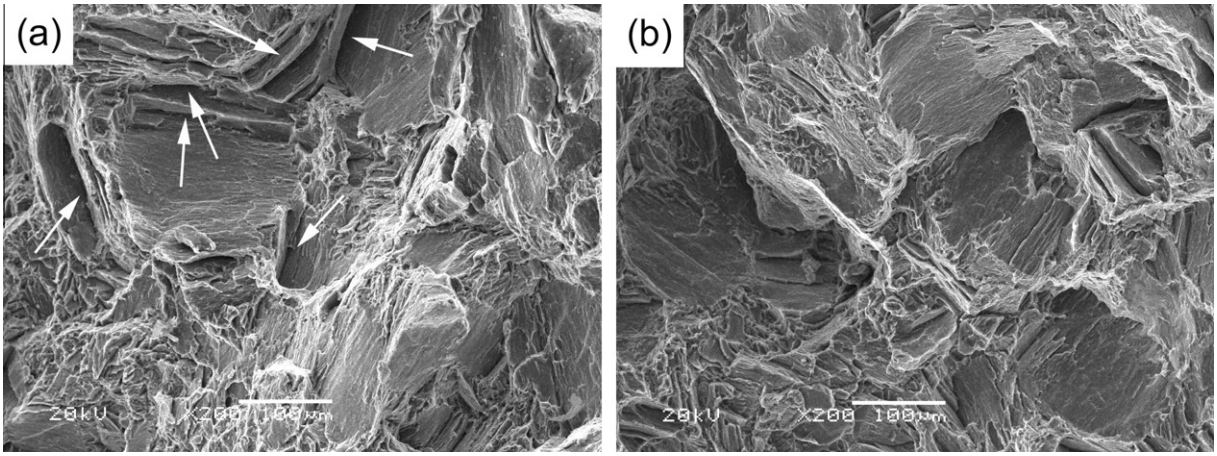

Fig. 11. Fractographs of the ZW21 alloys solutionized at 525 °C for (a) 1 h and (b) 4 h.

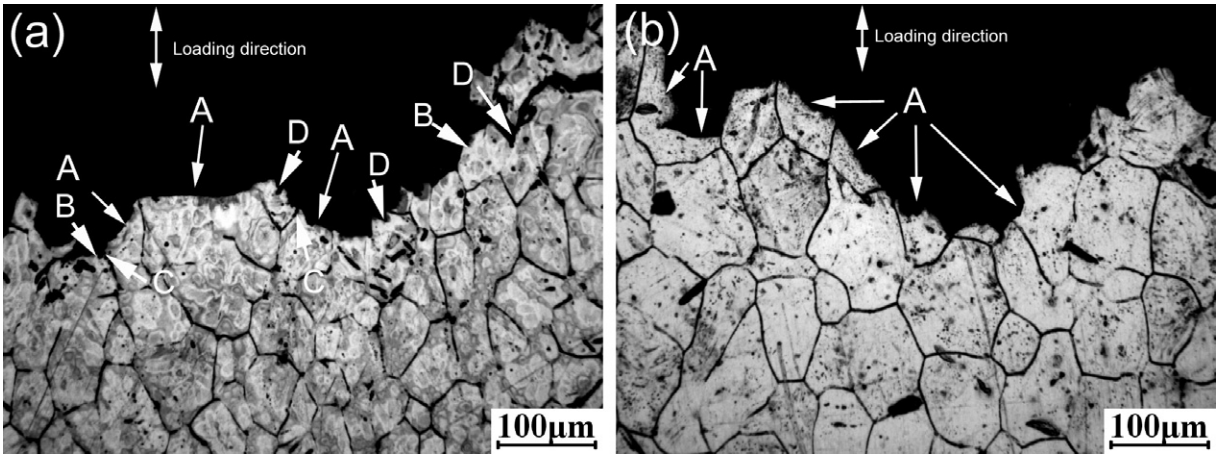

Fig. 12. Microstructures taken near the fracture surfaces along the longitudinal direction of tensile bars of the ZW21 alloys solutionized at 525 °C for (a) 1 h and (b) 4 h.

not completely transform into the α-Mg phase in a short time and they may partially disintegrate into small-sized W particles. In addition, the concentrations of Y and Nd in the primary α-Mg phase surrounding the eutectic W phase must significantly increase due to the partial dissolution of W phase. In some local sites, the concentrations of these two elements possibly exceed their saturation levels and thus some small W particles can precipitate again. Driving by decreasing the interfacial energy of W /α-Mg, the small-sized W particles then coarsen and agglomerate to form the flower-shaped structures.

As the solution treatment is further continued, the W phase particles gradually dissolve due to composition homogenization and then the flower-shaped structures disappear (comparing Fig. 7c and e or d and f). After being heated for 4 h, only some black particles distribute at the grain boundaries (Fig. 7e) and they cannot dissolve during the subsequent solution (Fig. 7g and h). The XRD result shows that the W phase has completely disappeared after being solutionized for 4 h (Fig. 8). Therefore, similar to the effect of solution temperature discussed in above section, the un-dissolved black particles should be MgSnCa particles. The MgSnCa particles and α-Mg grains also coarsen during the subsequent solution (comparing Fig. 7e and g or f and h).

Fig. 10 gives the variations of mechanical properties with solution time. It can be seen that the UTS, elongation and hardness run

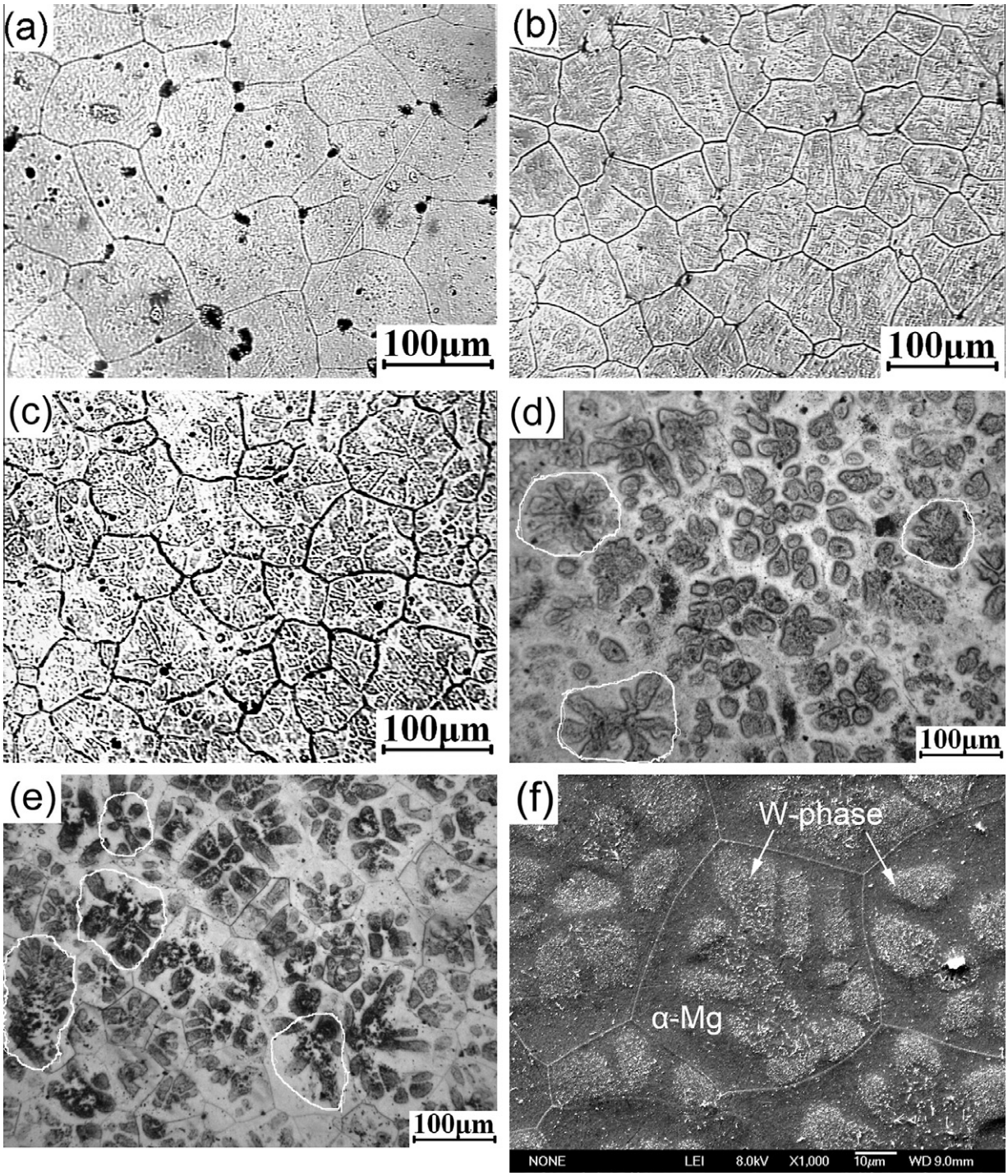

Fig. 13. Microstructures of the solutionized (at 525 °C for 4 h) ZW21 alloys after being aged at 250 °C for (a) 2 h, (b) 4 h, (c) 6 h, (d) 8 h, (e) 24 h and (f) 72 h.

in a same tendency with the time, they all increase with the time and are up to their maximum values when heated for 4 h (the UTS, elongation and hardness increase from 205 MPa, 18.25% and 50.59 HV of the as-cast alloy to 223 MPa, 26.5% and 52.28 HV, respectively), and then continuously decrease and finally tend to a steady state after 40 h. As discussed above, the interdendritic W phase gradually dissolves as the solution treatment proceeds and has completely disappeared when solutionized for 4 h. So its harmfulness to the mechanical properties is reduced and solution strengthening is improved, and thus the mechanical properties are enhanced and reach the maximum values when the W phase disappears. As the solution time is further prolonged, the main behavior is the coarsening of α-Mg grains and MgSnCa particles, which results in the decline of the mechanical properties. After the alloy experiences a period in which the coarsening runs rapidly and the phase interfacial energy decreases to a small degree, it will enter into another period in which the coarsening slowly runs. The results show that the microstructure does not obviously change after being heated for 40 h, which should be the main reason that the mechanical properties basically maintain constants after this time.

The fracture of the as-cast ZW21 alloy belongs to quasi-cleavage regime and the fracture surface is composed of dimples and facets. The dimples occupy the relatively large proportion of the surface and the facet size is quite small. During the initial stage of solution treatment, the eutectic W phase dissolves rapidly. But the composition of the α-Mg should be very heterogeneous, such as the formation of flower-shaped structures composed by W phase particles. So it can be expected that the deformation harmony of the α-Mg grains with such a composition distribution is very poor and they frequently fracture in a cleavage regime with obvious fragile characteristics. Consequently, many large cleavage facets with smooth surface are formed (Fig. 11a). As shown by Fig. 12a, these facets are originated from transgranular fracture (marked by A). In addition, some W phase particles still exist between the grains (Fig. 7c). So grain debonding can also be occasionally found and the debonding areas are relatively large (marked by B in Fig. 12a). Also due to the partial debonding (shown by C) and the grooves resulted from fragile cleavage fracture (shown by D), there are many cracks on the fracture surface (marked by arrows in Fig. 11a).

As the solution proceeds, the deformation harmony of the α-Mg grains should be improved due to composition homogenization. So the cleavage fracture with fragile characteristics is restrained and that with ductile characteristics is enhanced. Fig. 11b shows that the facet surfaces on the fracture surface of the alloy heated for 4 h are not smooth and some plastically deformed wrinkles are on them. Furthermore, the grain debonding cannot be found due to the disappearance of the interdendritic W phase and cracks basically propagate across the grains (marked A in Fig. 12b). When the solution time is further prolonged, for instance, when heated for 12 h, the facet size is further reduced and dimple characteristics are further enhanced due to the composition homogenization (Fig. 5c). That is to say the proportion of ductile fracture in the quasi-cleavage regime increases as the solution time increases. Moreover, the grain debonding is also rarely found. These changes should appear to be beneficial for improving mechanical properties. But the coarsening of α-Mg grains and MgSnCa particles is harmful to mechanical properties. The present results indicate that the disadvantage from the coarsening is larger than the benefit from the composition homogenization. During the subsequent solution, the most obvious event is still the coarsening of these two phases, especially the exceptional growth of some α-Mg grains (Fig. 7g). This growth must worsen the deformation harmony of α-Mg grains and the coarsening of MgSnCa particles certainly lead the grain boundaries to locally debond. So the facets with smooth surface gradually appear again and their area also increases. All of these result in the formation of fracture surface similar to that of

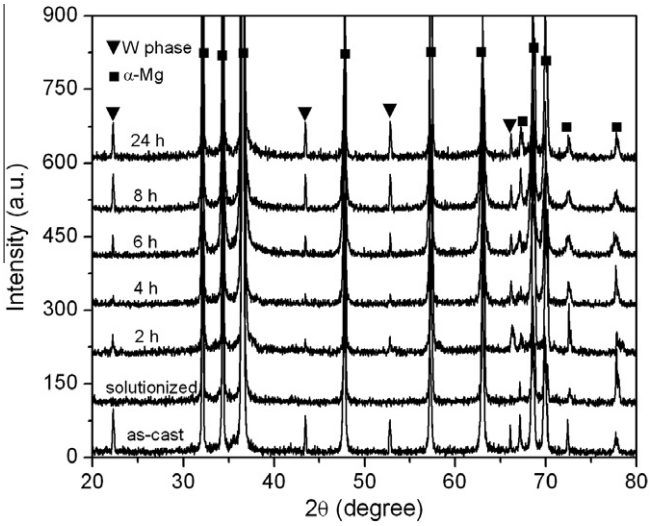

Fig. 14. XRD diffractograms of the solutionized (at 525 °C for 4 h) ZW21 alloys after being aged for different durations.

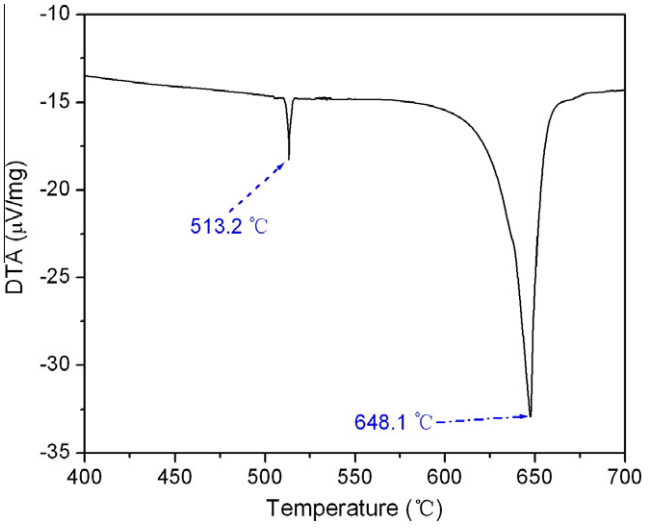

Fig. 15. DTA curve of the solutionized (at 525 °C for 4 h) ZW21 alloy after being aged for 24 h at 250 °C.

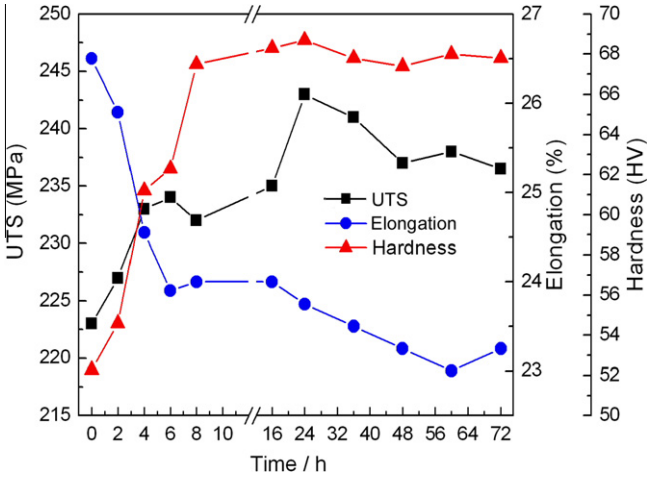

Fig. 16. Variations of mechanical properties of the solutionized (at 525 °C for 4 h) ZW21 alloy with aging time.

the alloy solutionized at the high temperature of 545 °C, the surface has sugar crystal-like characteristics (Fig. 5d). Namely, the quasi-cleavage fracture gradually evolves into the cleavage fracture as the solution time increases. In addition, the proportion of local grain debonding also increases. But when the time is over 40 h, both the cleavage fracture regime and crack propagation path do not change because the coarsening of the α-Mg grains and MgSnCa particles is very slow after this time.

Summarily, as the solution proceeds, the interdendritic W phase gradually dissolves into the α-Mg grains, the alloy's mechanical properties are improved and up to peak values when the alloy is heated for 4 h at 525 °C. Correspondingly, the dimple proportion on the facture surface increases and the grain debonding is restrained although the quasi-cleavage fracture regime does not change. Subsequently, the composition should be further homogenized, but both the α-Mg grains and MgSnCa particles grow up. So the mechanical properties then decrease although some characteristics on the fracture surfaces that are seemly beneficial for improving mechanical properties become more and more obvious. When the solution time is over 12 h, the fracture regime gradually changes from quasi-cleavage to cleavage due to the coarsening of α-Mg grains and MgSnCa particles. Simultaneously, grain debonding appears again and also become more and more obvious.

3.3. Effects of aging treatment on microstructure and mechanical properties

It is known that the mechanical properties of the ZW21 alloy are up to peak values after being solutionized for 4 h at 525 °C. So this solution technique is appropriate for this alloy, and thus the alloy heated using this regime is taken to study the effects of aging treatment on the microstructure and mechanical properties. Fig. 13 gives the microstructures of the alloys aged for different times at 250 °C. It shows that innumerable fine particles dispersively precipitate in the α-Mg matrix during the initial aging stage (Fig. 13a). Then the precipitates gradually coarsen and agglomerate to form flower-shaped structures (Fig. 13b–e). The XRD results indicate that the peaks of W phase appear and its intensity increases as the aging time extends (Fig. 14), which imply that the precipitates should be the W phase. In addition, an endothermic peak at 513 °C appears in the DTA curve of the alloy aged for 4 h (Fig. 15). It is known that this peak corresponds to the melting of eutectic W phase [5]. That is the W phase has formed when the alloy is aged for 4 h, which further demonstrates that the precipitates are the W phase.

The formation of the flower-shaped structures in the aged alloys indicates that the distribution of solute atoms in the solutionized alloy is not very homogeneous. The solute concentrations in the original inter-arm regions should be higher than those in the other regions, and thus the number and amount of the precipitates in the former regions must be higher than those in the other regions. During the subsequent aging, the precipitates in one original inter-arm region will agglomerate into one petal driving by decreasing the W/α-Mg interfacial energy. Through comparing Fig. 7c with Fig. 13d, e and f, it can be found that the petals of some flower-shaped structures in the aged alloys are connected each other at the central region (marked by circles in Fig. 13d, e and f) while those in the solutionized alloy are all separate (Fig. 7c and d). This difference should be attributed to the composition homogenization resulted from the subsequent solution treatment. As shown by

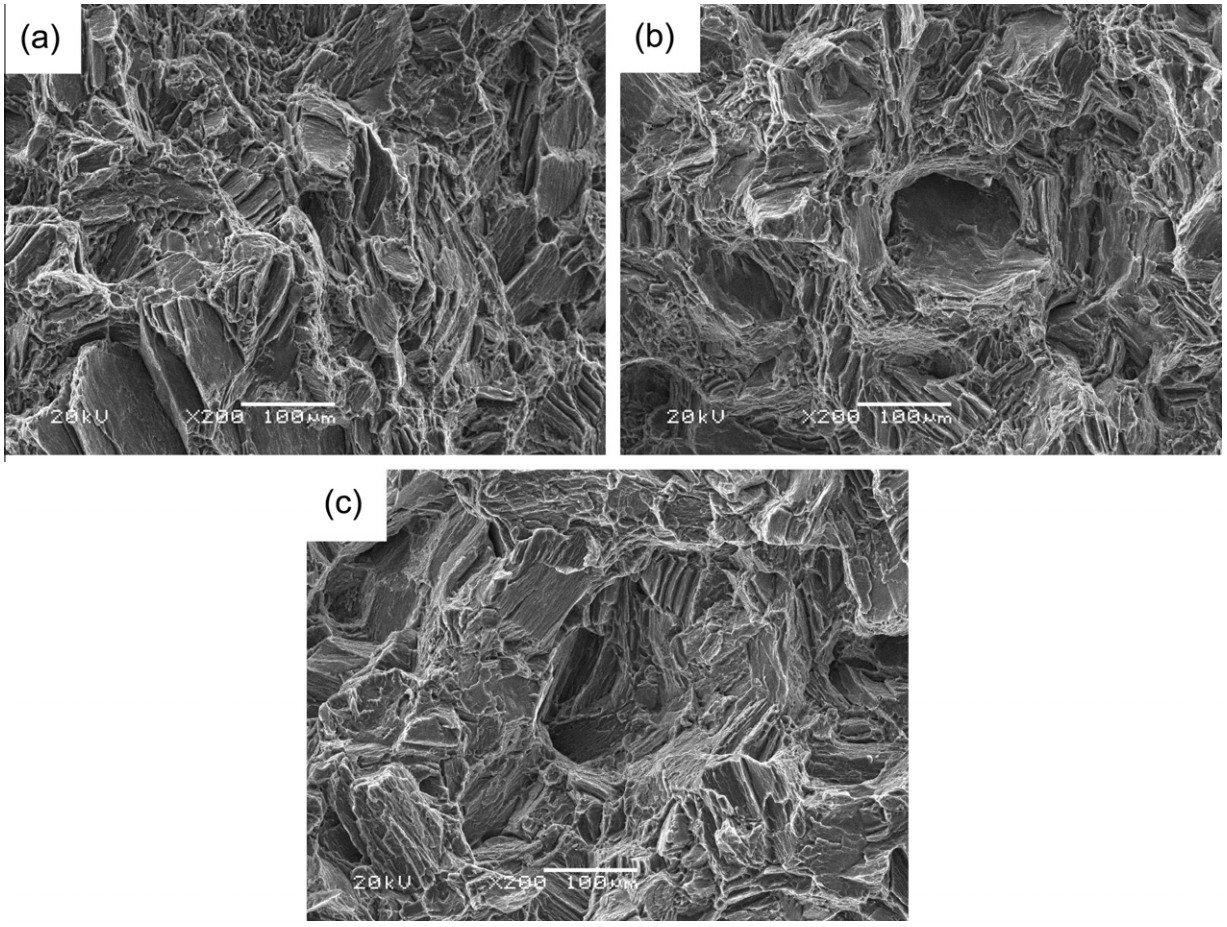

Fig. 17. Fractographs of the solutionized (at 525 °C for 4 h) ZW21 alloy after being aged at 250 °C for (a) 2 h, (b) 24 h and (c) 72 h.

Fig. 13a and b, the precipitates dispersively distribute in the whole grains, but only the number and amount in the original inter-arm regions are higher than those in the other regions. So it can be expected that the sites of the petals formed during the subsequent aging may be slight away from the original inter-arm regions and some of the petals may connect each other. But for the solutionized alloy, the petals exactly form at the inter-arm regions and they are separated by the primary α-Mg phase. In addition, it should be noted that the mechanical properties are the highest although the composition is not very homogeneous for the alloy solutionized for 4 h at 525 °C. Namely, this solution technique is appropriate if the mechanical properties are taken as the criterion for evaluating solution technique.

Fig. 16 gives the variations of mechanical properties with the solution time. It shows that the elongation continuously decreases as the time extends. But the UTS and hardness first increase and reach their maximum values at 24 h (the UTS and hardness increase from 223 MPa and 52.28 HV of the solutionized alloy to 243 MPa and 68.7 HV respectively), and then slowly decrease. It is well known that precipitate strengthening is the main reason that aging treatment improves mechanical properties of an alloy. Simultaneously, the elongation always decreases due to the precipitates' blocking to the movement of dislocations, twins or slip. It can be expected that this blocking role can decrease the deformation harmony of grains, and thus enhance the cleavage fracture with brittle characteristics. In addition, the precipitates can hinder the propagation of cracks and this hindering effect will also be enhanced as the precipitate size increases. The former may produce the cleavage facets with flat surface and the later may decrease the area of cleavage facets due to the frequent change of crack propagation directions. So as shown by the fracture surface of the alloy aged for 2 h (Fig. 17a), the facets are smaller but flatter than those of the solutionized alloy (comparing Figs. 11b and 17a). Fig. 18a shows that the grain debonding can be frequently seen for the alloy aged for 2 h (marked by A). This implies that the precipitates at the grain boundaries impair the grain bonding strength because the grain boundaries are the sites where the W precipitates preferentially form and the W phase is harmful for grain bonding strength.

As the aging time increases, the number and amount, especially the size of the precipitates also increase. So the facet size correspondingly decreases due to the enhanced hindering effect of the large-sized precipitates to crack propagation (comparing Fig. 17a and b). In addition, the precipitates gradually agglomerate into the flower-shaped structures within the grains, and thus the grain bonding strength is improved and the grain debonding is rarely found (Fig. 18b). As to why the precipitates agglomerate within the grains, but not at the grain boundaries, the reasons need to be further verified. It is just the precipitate strengthening and improved grain bonding strength that the alloy aged for 24 h has the highest UTS and hardness. As the aging time is further elongated, the microstructure including grain size and morphology of the flower-shaped structures does not obviously change (comparing Fig. 13e and f). But it can be expected that the W precipitates should further coarsen and agglomerate, which may lead the deformation to be more incompatible and the change frequency

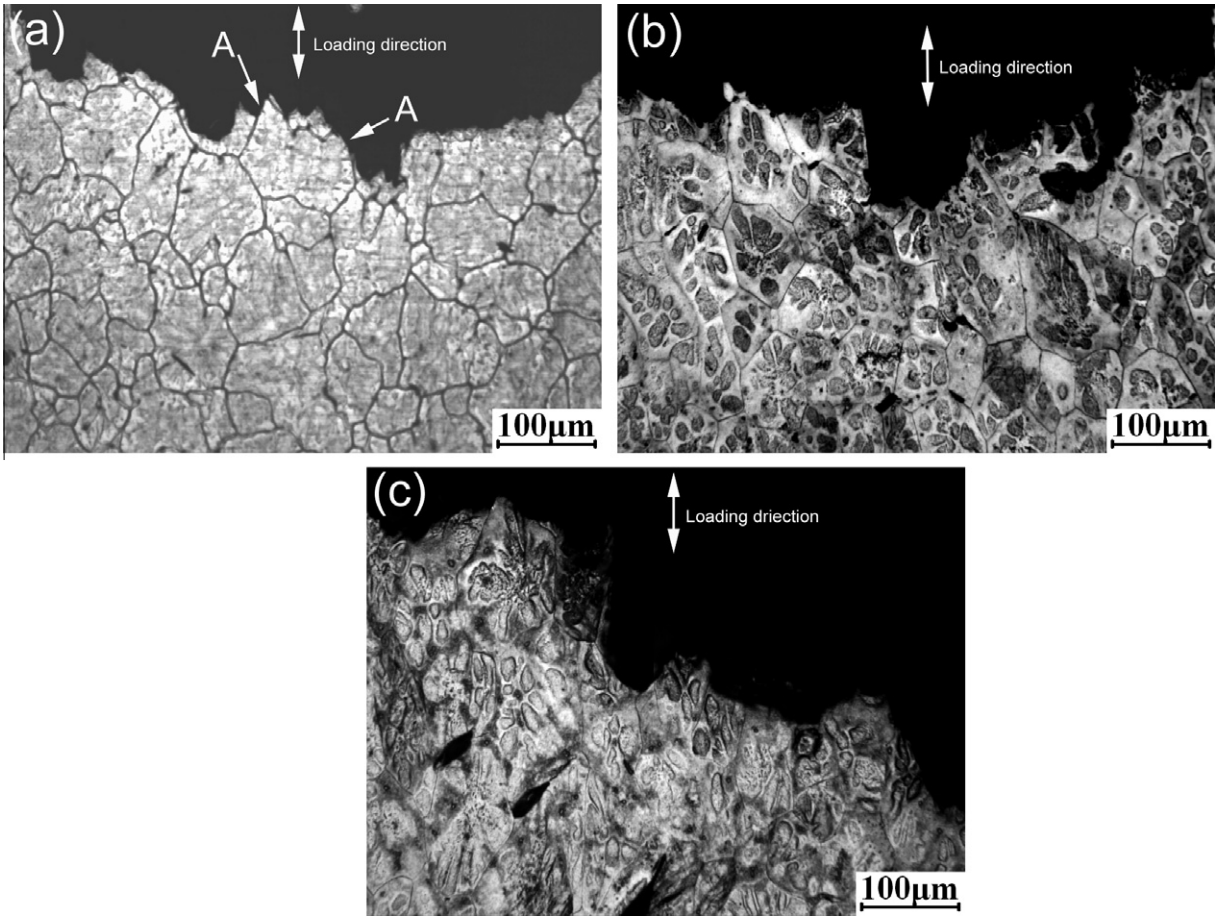

Fig. 18. Microstructures taken near the fracture surfaces along the longitudinal direction of tensile bars of the solutionized (at 525 °C for 4 h) ZW21 alloy after being aged at 250 °C for (a) 2 h, (b) 24 h and (c) 72 h.

of crack propagation direction to decrease. So the cleavage facets with relatively large size appear again (Fig. 17c). But Fig. 18c indicates that the coarsening and agglomeration of the precipitates do not change the path of crack propagation, i.e. cracks still propagate across the grains. Based on this discussion, it can be easily understand the continuous decrease of the mechanical properties after 24 h. Finally, it should be noted that the aging treatment can not alter the fracture regime of quasi-cleavage although some changes occur for the size and morphology of cleavage facets (Fig. 17).

Therefore, it can be concluded that the precipitate phase during aging is the W phase for the solutionized ZW21 alloy. The precipitates then coarsen and agglomerate into flower-shaped structures during the subsequent aging. These precipitate behaviors cause the elongation to continuously decrease, but lead the UTS and hardness to increase. The increase of UTS and hardness should be contributed to the hindering effect of the coarsened precipitate particles to crack propagation and the improved grain bonding strength. The grain bonding strength is improved by the agglomeration of W precipitates at grain boundaries inside the grains. When the aging time is over 24 h, both the UTS and hardness then decrease due to the further coarsening and agglomeration of the precipitates. Correspondingly, the size of cleavage facets first decreases and then increases again after being aged for 24 h. This change is attributed to the variations of the deformation harmony, grain bounding strength and hindering effect to crack propagation that result from the precipitate behaviors. The proportion of grain debonding in the crack propagation paths also changes a little due to the variation of grain bonding strength,

4. Conclusions

(1) The interdendritic eutectic W phase with discontinuous laths and large-sized pools in the as-cast ZW21 alloy is harmful to its mechanical properties. Solution heat treatment can dissolve the W phase into the primary α-Mg and thus improve the mechanical properties. Subsequent aging treatment generates the flower-shaped structures composed of W phase particles within the grains and leads the mechanical properties to be further improved.

(2) A proper heat treatment technique is achieved, solution for 4 h at 525 °C and subsequent age for 24 h at 250 °C. The UTS, elongation and hardness can be increased by this technique from 205 MPa, 18.25% and 50 HV to 243 MPa, 23.75% and 68.7 HV, respectively.

(3) The bonding strength of W/α-Mg interface is quite strong because the interface debonding is rarely found. The grain debonding is resulted from the propagation of cracks along the interdendritic W phase. So a proper solution treatment can change the fracture from the mixture of transgranular and intergranular modes to a completely transgranular mode. Higher solution temperature or longer solution time will generate a small proportion of intergranular fracture again due to the grain growth and MgSnCa particle coarsening.

(4) As the solution temperature rises from 505 °C to 545 °C, the fracture regime changes from the quasi-cleavage of the as-cast alloy in turn to cleavage (505 °C), quasi-cleavage (525 °C) and cleavage (545 °C). But as the solution time at 525 °C increases, the regime changes from the quasi-cleavage to complete cleavage. All of these changes are attributed to the variation of deformation harmony resulted from composition homogenization, grain growth and MgSnCa particle coarsening.

(5) During the initial aging period, numerous fine W precipitates dispersively distribute in α-Mg matrix, but the mechanical properties are not so high. When the precipitates agglomerate inside the grains, the mechanical properties, especially the UTS, are up to the maximum values due to the improvement of grain bonding strength.

(6) The aging treatment does not change the fracture regime of quasi-cleavage, but can alert the size of cleavage facets and the proportion of grain debonding in the crack propagation.

Acknowledgement

The authors wish to express thanks to financial support from the National Basic Research Program of China (Grant No. G2010CB635106), the Program for New Century Excellent Talents in University of China (Grant No. NCET-10-0023) and the Program for Hongliu Outstanding Talents of Lanzhou University of Technology.

References

[1] G. Hanko, H. Antrekowitsch, P. Ebner, JOM 2 (2002) 51–54.
[2] J.Y. Lee, D.H. Kim, H.K. Lim, D.H. Kim, Mater. Lett. 59 (2005) 3801–3805.
[3] Z.H. Huang, S.M. Liang, R.S. Chen, E.H. Han, J. Alloys Comp. 468 (2009) 170–178.
[4] D.K. Xu, W.N. Tang, L. Liu, Y.B. Xu, E.H. Han, J. Alloys Comp. 432 (2007) 129–134.
[5] T.J. Chen, W. Wang, D.H. Zhang, Y. Ma, Y. Hao, Mater. Des. (2012), http://dx.doi.org/10.1016/j.matdes.2012.08.040.
[6] Q. Li, Q. Wang, Y. Wang, X. Zeng, W. Ding, J. Alloys Comp. 427 (2007) 115–123.
[7] J.F. Nie, B.C. Muddle, Acta Mater. 48 (2000) 1691–1703.
[8] J. Chen, Z. Chen, H. Yan, F. Zhang, K. Liao, J. Alloys Comp. 461 (2008) 209–215.
[9] M. Qian, A. Das, Scr. Mater. 54 (2006) 881–886.
[10] S.-S. Li, B. Tang, D.-B. Zeng, J. Alloys Comp. 437 (2007) 317–321.
[11] M. Zhu, Y.S. Sun, F. Xue, Jiangsu Metall. 6 (2002) 1–5.
[12] D.K. Xu, E.H. Han, Lu Liu, Y.B. Xu, Metall. Mater. Trans. A 40 (2009) 1728–1740.
[13] S.W. Xu, M.Y. Zheng, S. Kamado, K. Wu, G.J. Wang, X.Y. Lv, Mater. Sci. Eng. A 528 (2011) 4055–4067.
[14] D.H. Bae, S.H. Kim, D.H. Kim, W.T. Kim, Acta Mater. 50 (2002) 2343–2356.
[15] A. Singh, A.P. Tsai, Scr. Mater. 53 (2005) 1083–1087.
[16] A. Singh, H. Somekawa, T. Mukai, Mater. Sci. Eng. A 528 (2011) 6647–6651.
[17] D.K. Xu, L. Liu, Y.B. Xu, E.H. Han, Mater. Sci. Eng. A 420 (2006) 322–332.
[18] D.K. Xu, L. Liu, Y.B. Xu, E.H. Han, J. Alloys Comp. 426 (2006) 155–161.
[19] J. Wang, S. Gao, P. Song, X. Huang, Z. Shi, F. Pan, J. Alloys Comp. 509 (2011) 8567–8572.
[20] J. Wang, P. Song, S. Gao, X. Huang, Z. Shi, F. Pan, Mater. Sci. Eng. A 528 (2011) 5914–5920.
[21] J. Wang, P. Song, S. Gao, Y. Wei, F. Pan, J. Mater. Sci. 47 (2012) 2005–2010.
[22] D.K. Xu, L. Liu, Y.B. Xu, E.H. Han, Mater. Sci. Eng. A 443 (2007) 248–256.
[23] D.K. Xu, W.N. Tang, L. Liu, Y.B. Xu, E.H. Han, J. Alloys Comp. 461 (2008) 248–252.
[24] A. Singh, M. Watanabe, A. Kato, A.P. Tsai, Scr. Mater. 51 (2004) 955–960.
[25] W.J. Kim, S.I. Hong, K.H. Lee, Met. Mater. Int. 16 (2010) 171–174.
[26] H. Liu, Y. Chen, H. Zhao, S. Wei, W. Gao, J. Alloys Comp. 504 (2010) 345–350.
[27] B.H. Kim, K.C. Park, Y.H. Park, I.M. Park, Mater. Sci. Eng. A 528 (2011) 808–814.
[28] B.H. Kim, S.M. Jo, Y.C. Lee, Y.H. Park, I.M. Park, Mater. Sci. Eng. A 535 (2012) 40–47.
[29] Y. Zhang, X. Zeng, L. Liu, C. Lu, H. Zhou, Q. Li, Y. Zhu, Mater. Sci. Eng. A 373 (2004) 320–327.